Reliability of base-isolated structures with sliding hydromagnetic bearings considering stochastic ground motions

L.C. Ding, R. Van Coile & R. Caspeele
Department of Structural Engineering, Ghent University, Ghent, Belgium

Y.B. Peng
State Key Laboratory of Disaster Reduction in Civil Engineering, Tongji University, Shanghai, P.R. China
Shanghai Institute of Disaster Prevention and Relief, Tongji University, Shanghai, P.R. China

J.B. Chen
State Key Laboratory of Disaster Reduction in Civil Engineering, Tongji University, Shanghai, P.R. China
College of Civil Engineering, Tongji University, Shanghai, P.R. China

ABSTRACT: Stochastic seismic response analysis and reliability assessment of a base-isolated structure with sliding hydromagnetic bearings are performed combining the probability density evolution method and the stochastic function model of seismic ground motions. The reliability assessments are based on the extreme value distribution of the inter-story drifts of the base-isolated structure. Compared with the responses of the base-fixed structure, the superstructure of the base-isolated structure almost behaves like a rigid body. The sliding hydromagnetic bearing is efficient in reducing the responses by one degree of seismic intensity. Finally, the dynamic reliability of the base-isolated structure is evaluated, which provides an index for decision making in practice.

1 INTRODUCTION

As an efficient technique of structural control, base isolation is widely used in the response mitigation and performance enhancement of structural seismic hazard reduction (Narasimhan et al. 2006, Chen et al. 2007, Saaed et al. 2015). Modern isolation technologies originated in the 1970s, which mainly includes three kinds of technologies: the laminated rubber bearing, the friction sliding bearing, and the curved surface slider (Villaverde 2017). These technologies, however, have some limitations. For instance, the laminated elastomeric bearings show a considerable degradation of mechanical properties due to wear after obvious sliding. The purely flat sliding bearings lack a restoring force and provide low damping, which might lead to unacceptable large sliding displacements. The restoring forces of curved surface sliders increase linearly with the sliding displacements and result in additive vibration along the vertical structure.

Recently, a novel base isolation, the sliding hydromagnetic bearing, has been proposed (Villaverde 2017). It offers several technical benefits: lowering of the friction between bearing and base plate, restoring force pushing the bearing back toward the initial position, and a displacement constraint which prevents the bearing from sliding off the base plate. In addition, the sliding hydromagnetic bearing has been further studied with quasi-static tests (Peng et al. 2017) and numerical performance evaluations of the applicability and efficiency of this technology (Peng et al. 2018).

Evaluating the failure probability of stochastic dynamic systems is particularly challenging. The Probability Density Evolution Method (PDEM) has been presented in literature (Chen et al. 2007) as an efficient method to deal with dynamic structural problems. In addition, the stochastic function model of seismic ground motions whose parameters are identified using real ground motion records from the NGA West2 database of PEER (Ding et al. 2018a, Ding et al. 2018b) is employed to obtain the stochastic ground motions.

In this contribution, the dynamic reliability of a base-isolated structure with sliding hydromagnetic bearings is evaluated using the Probability Density Evolution Method (PDEM). Meanwhile, three hundreds representative artificial seismic ground motions are generated using the stochastic function model of seismic ground motions. The stochastic seismic response analyses are also implemented with a base-fixed structure to compare with the responses of the base-isolated structure. Finally, the reliabilities are evaluated based on the extreme value distribution of inter-story drifts of the based-isolated structure.

2 THE SLIDING HYDROMAGNETIC BEARING

Sliding isolation, as one of the base isolation approaches, has demonstrated its value in seismic hazard mitigation. Its primary principle is shifting the structural period from the dominant period of the seismic ground motions by deploying devices, which also

acts as an energy dissipater, between the superstructure and foundation to decouple the motion of the superstructure from that of the ground. The technical and economic advantages of base-isolated structures have been well-proven in practice (Guo et al. 2009).

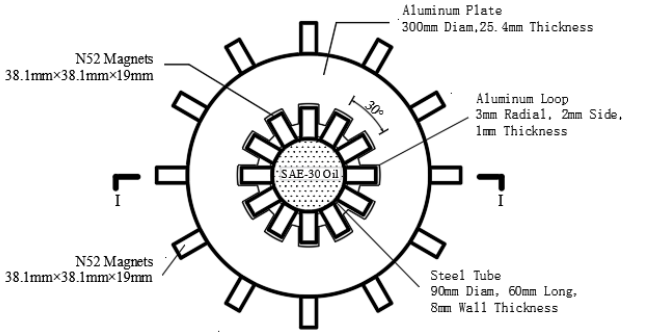

(a) plan view

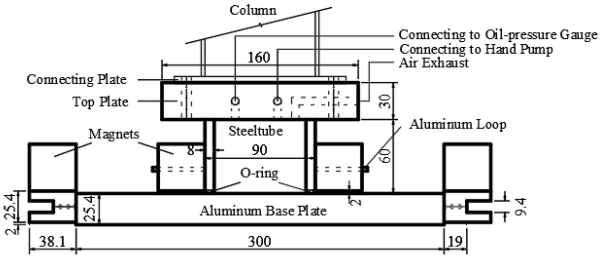

(b) side view I-I

Figure 1. Design diagram of sliding hydromagnetic isolator.

As shown in Figure 1, a novel base isolation system based on the use of hydromagnetic bearings sliding over circular aluminum base plates and sintered neodymium-iron-boron permanent magnets has been proposed by Villaverde (2017). These bearings comprise steel tubes with a pressurized internal fluid and attached permanent magnets, and slide over aluminum base plates also with attached permanent magnets. They minimize the friction between bearings and base plates, generate damping forces that reduce the bearings displacements to practical levels, and introduce restoring forces and displacement constraints.

In addition, the sliding hydromagnetic isolators were designed, fabricated and tested experimentally to assess its performance. Numerical simulations were carried out for quantifying the repulsive, damping, and friction forces involved (Peng et al. 2017). Moreover, for a verification of efficiency of the sliding hydromagnetic bearing, performance evaluations of base-isolation system with sliding hydromagnetic bearings were carried out. The formula for modeling the restoring force named as the power-function model is as (Peng et al. 2018)

$$F(x,\dot{x}) = 3661f^{-0.87}\mathrm{sgn}(\dot{x})|\dot{x}|^{1.87} + 2\sinh(79x) + \mu N\mathrm{sgn}(\dot{x}) \quad (1)$$

where x and $\dot{x}$ denote the deformation of the isolated layer and the velocity of the sliding bearing, respectively; f denotes a parameter associated with frequency, which can be selected as the characteristic frequency of the isolated structure for the seismic simulation (Peng et al. 2018); μ denotes the coefficient of friction, which is assigned a value of 0.049 according to the experimental results (Peng et al. 2017); N denotes the vertical load placed on the cap plate of the device; sinh(·) denotes the hyperbolic sine function; and sgn(·) denotes the signum function.

3 THE STOCHASTIC FUNCTION MODEL OF SEISMIC GROUND MOTIONS

Stochastic earthquake ground motions play an important role in seismic response analysis and structural reliability evaluation (Boore 1983, Chen et al. 2007, Rezaeian & Der Kiureghian 2008). Considering non-stationarities both in the time and frequency domain, a stochastic function model of seismic ground motions is proposed (Wang & Li 2011, Ding et al. 2018a). The physical mechanisms of seismic ground motions, which include the randomness inherent in the source, propagation path and local site, have been considered as part of the model derivation. In this model, the seismic source is viewed as a spatial point where the seismic waves are generated. The seismic waves propagate along a one-dimensional path, and the local site is idealized as a one-degree-of-freedom filter.

As presented in Eq. (2), the model includes two terms, the former is the amplitude spectrum $A_R(\boldsymbol{\theta},\omega)$ and the latter is the phase spectrum $\Phi_R(\boldsymbol{\theta},\omega)$.

$$a_R(t) = -\frac{1}{2\pi}\int_{-\infty}^{+\infty} A_R(\boldsymbol{\theta},\omega)\cos[\omega t + \Phi_R(\boldsymbol{\theta},\omega)]\,d\omega \quad (2)$$

$$A_R(\boldsymbol{\theta},\omega) = \frac{A_0\omega\cdot e^{-K\omega R}}{\sqrt{\omega^2+(\tau)^{-2}}}\cdot\sqrt{\frac{1+4\xi_g^2\left(\frac{\omega}{\omega_g}\right)^2}{\left[1-\left(\frac{\omega}{\omega_g}\right)^2\right]^2+4\xi_g^2\left(\frac{\omega}{\omega_g}\right)^2}} \quad (3)$$

$$\Phi_R(\boldsymbol{\theta},\omega) = \arctan\left(\frac{1}{\tau\omega}\right) - R\cdot\ln[a\omega + 1000b + 0.1323\sin(3.78\omega) + c\cos(d\omega)] \quad (4)$$

where $a_R(t)$ is the acceleration time history of seismic ground motion; $\boldsymbol{\theta}$ is a vector of stochastic parameters; R is the propagation distance; A_0 and τ are the Brune source parameters; K is the attenuation parameter; a, b, c and d are the parameters of an empirical frequency-wave number formula; ξ_g and ω_g are the equivalent damping ratio and equivalent predominate circular frequency of local site, respectively (Ding et al. 2018a).

In the following sections of this contribution, the physical parameters A_0, τ in the Brune source model and ξ_g, ω_g in the local site model are random variables. Meanwhile, the parameters from the wave number-frequency relationship and propagation distance (i.e. the Joyner-Boore distance) are a, b, c, d and R

which are also random variables. They are then denoted by $\boldsymbol{\theta} = [A_0, \tau, \xi_g, \omega_g, R, a, b, c, d]$. It is noted that A_0 affects the amplitude and τ, ξ_g, ω_g affect the shape of Fourier amplitude spectrum. In addition, all these parameters are regarded as independent random variables.

In this contribution, the parameters of large magnitude and long distance group of site II, which are classified based on a cluster analysis of ground motion records collected from the NGA West2 database of PEER, are implemented according to the literature. A_0, τ, R, a, c, and d satisfy a lognormal distribution, the mean values of the distributions are -1.2345, -1.7412, 3.4712, 1.6495, 1.3116 and -1.0764, respectively; the standard deviations are 0.8903, 1.6729, 1.2868, 0.8885, 0.8540 and 0.8109, respectively. ξ_g and ω_g satisfy a Gamma distribution, the distribution of which the shape parameters are 2.8792 and 2.2370, respectively; the scale parameters are 0.1665 and 8.3990, respectively. Finally, b satisfies the normal distribution, with a mean and standard deviation of 8.6314 and 3.7139, respectively. (Ding et al. 2018a)

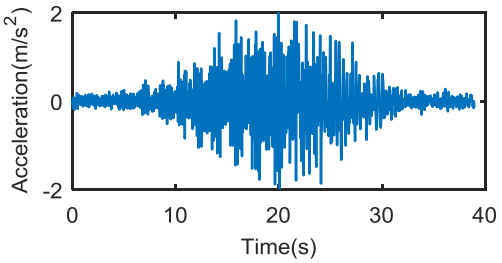

(a) The artificial ground motion sample 123

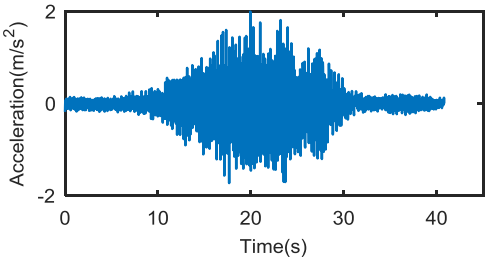

(b) The artificial ground motion sample 202

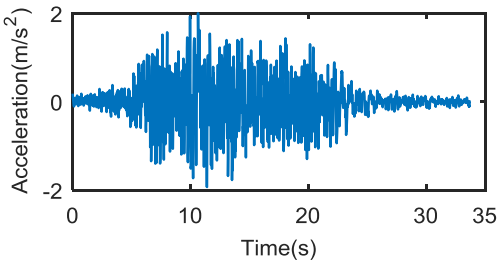

(c) The artificial ground motion sample 272

Figure 2. Representative time histories of artificial ground motions.

In total, three hundreds representative artificial seismic ground motions with corresponding assigned probabilities are generated using the GF discrepancy-based method (Chen et al. 2016) in this contribution. Three representative time histories of artificial ground motions are shown in Figure 2. The PGAs of all the records are normalized to 0.2g for the requirement of consistency. It is obvious that these artificial ground motions include randomness inherent in duration and non-stationarity in the time domain. In addition, the time step is 0.02s and the total time of the ground motions are processed to 90s by adding zeros after every sample for the reliability analysis by using the PDEM.

4 DYNAMIC RELIABILITY ASSESSMENT BASED ON THE EXTREME VALUE DISTRUTION

4.1 *Foundations of the Probability Density Evolution Method* (*PDEM*)

With discretization techniques such as the finite element method, the equation of motion of a stochastic base-isolated structure subjected to earthquake is denoted as

$$\mathbf{M}\ddot{\mathbf{X}} + \mathbf{G}(\mathbf{X}, \dot{\mathbf{X}}) = -\mathbf{M}\mathbf{I}\ddot{x}_g(\boldsymbol{\Theta}, t) \tag{5}$$

where, $\mathbf{M}$ is an n by n mass matrix; $\mathbf{G}(\cdot)$ is the internal forces of the structure including the damping forces and restoring forces; $\mathbf{I}$ is an n-order column vector with all elements equal to unity; $\ddot{x}_g$ is the ground time history; and $\boldsymbol{\Theta}=(\theta_1,\theta_2,\ldots,\theta_s)$ is a random vector characterizing the randomness involved in the ground motions. The joint pdf $p_\Theta(\theta)$ is identified in the previous section. $\mathbf{X}=(X_1,X_2,\ldots,X_n)^T$ is an n by 1 relative displacement vector, over-dots denote differentiation with respect to t. In addition, both the initial velocity and initial displacement are zero. The solution $\mathbf{X}$, which can be the displacements associated with the stochastic dynamical system at any point, for the dynamical system is

$$\mathbf{X} = \mathbf{H}(\boldsymbol{\Theta}, t) \tag{6}$$

$$\dot{\mathbf{X}} = \mathbf{h}(\boldsymbol{\Theta}, t) \tag{7}$$

where $\mathbf{h} = \partial\mathbf{H}/\partial t$. It is noted that the randomness involved in $\mathbf{X}(t)$ results completely from $\boldsymbol{\Theta}$. Considering the preservation of probability, the system ($\mathbf{X}(t)$, $\boldsymbol{\Theta}$) is a probability preserved system. Therefore, the generalized density evolution equation (GDEE) is obtained as

$$\frac{\partial p_{\mathbf{X}\boldsymbol{\Theta}}(x,\theta,t)}{\partial t} + \dot{X}(\theta,t)\frac{\partial p_{\mathbf{X}\boldsymbol{\Theta}}(x,\theta,t)}{\partial x} = 0 \tag{8}$$

Then the joint density of $\mathbf{X}(t)$ can be given by

$$p_{\mathbf{X}}(x,t) = \int_{\Omega_\Theta} p_{\mathbf{X}\boldsymbol{\Theta}}(x,\theta,t)\, d\theta \tag{9}$$

where Ω_Θ is distribution domain of $\boldsymbol{\Theta}$. The methodology for tackling stochastic dynamical problems though solving the GDEE is called the probability density evolution method (PDEM). Numerical solution of finite-difference method with total variation diminishing schemes (TVD) exhibits satisfactory per-

formances in the probability density evaluation analysis (Li & Chen 2009), and will be adopted in the present paper.

4.2 *Dynamic reliability assessment based on the extreme value distribution*

The main target of structural reliability analysis is to evaluate the probability of the structural response not exceeding the limit state. When the response doesn't exceed the limit state, the structure is in a safe state. If p_x is not time-dependent (i.e. static problem), the reliability P_s or failure probability P_f can be given by the integral of the joint pdf

$$P_{\mathrm{s}} = 1 - P_{\mathrm{f}} = \int_{\Omega_{\mathrm{s}}} p_{\mathrm{X}}(x)dx \tag{10}$$

where Ω_s is the safe domain.

When p_X is time-dependent, the dynamic reliability can be defined as

$$P_{\mathrm{s}} = \mathrm{P}\{X(t) \in \Omega_{\mathrm{s}}, t \in [0,T]\} \tag{11}$$

where $\mathrm{P}\{\cdot\}$ denotes the probability of the random event, $X(t)$ denotes the physical quantities of the structure. Eq. (11) is equivalent to

$$P_{\mathrm{s}} = \mathrm{P}\{W(\boldsymbol{\Theta}, t) \in \Omega_{\mathrm{s}}\} \tag{12}$$

where $W(\boldsymbol{\Theta}, t)$ is the extreme value of $X(t)$ over time interval $[0,T]$. For instance, it can be defined by

$$W(\boldsymbol{\Theta}, T) = \max_{t\in[0,T]} |X(\boldsymbol{\Theta}, t)| \tag{13}$$

The pdf of the extreme values defined by Eqs. (12) or (13) can be obtained by introducing the concept of virtual stochastic process (Chen & Li 2007). A virtual stochastic process is constructed as

$$Z(\tau) = \psi(W(\boldsymbol{\Theta}, T), \tau) = \phi(\boldsymbol{\Theta}, \tau) \tag{14}$$

which satisfies the conditions

$$Z(\tau)|_{\tau=0} = 0,\ Z(\tau)|_{\tau=\tau_c} = \psi(W(\boldsymbol{\Theta}, T), \tau_c) = \phi(\boldsymbol{\Theta}, \tau_c) = E(\boldsymbol{\Theta}, T) \tag{15}$$

where τ_c is a prescribe value. Then it is easy to note that Eq. (14) is in a form similar to Eq. (6). The GDEE is employed to get the pdf of $Z(\tau)$

$$p_{\mathbf{Z}}(z,\tau) = \int_{\Omega_{\boldsymbol{\Theta}}} p_{\mathbf{Z}\boldsymbol{\Theta}}(z,\theta,\tau)\, d\theta \tag{16}$$

Therefore, the pdf of W is then obtained as

$$P_W(w) = p_{\mathbf{Z}}(z = w, \tau)\,|_{\tau=\tau_c} \tag{17}$$

the reliability in Eq. (11) can then be evaluated by

$$P_{\mathrm{s}} = \mathrm{P}\{W(\boldsymbol{\Theta}, \tau) \in \Omega_{\mathrm{s}}\} = \int_{\Omega_{\mathrm{s}}} p_W(w)dw \tag{18}$$

It should be noted here that the dynamical reliability evaluation becomes a problem of one-dimensional integration of the extreme value distribution.

The form of $\varphi(\cdot)$ and $\phi(\cdot)$ is arbitrary when Eq. (15) is satisfied. In this contribution, the virtual stochastic process in Eq. (14) is realized by

$$Z(\tau) = \psi(W(\boldsymbol{\Theta}, T), \tau) = W(\boldsymbol{\Theta}, T)\sin(w\tau) \tag{19}$$

in which w=2.5π, τ_c=1.

5 RELIABILITY OF A BASE-ISOLATED STRUCTURE WITH SLIDING HYDROMAGNETIC BEARINGS

5.1 *Base-isolated structure with sliding hydromagnetic bearings*

As shown in Figure 3(a), the design and dimensions of the sliding hydromagnetic bearing are based on the 1/4-scale structure. The scaled structure is a six-floor and two-span steel frame with concrete slabs, with plan size of 2m×3m and height of 6×0.9m=5.4m. The design parameters are specified according to the seismic resistance design code: the seismic intensity of degree 8 with a basic peak ground acceleration (PGA) of 0.2g, soil type II, and the design characteristic period of 0.57s.

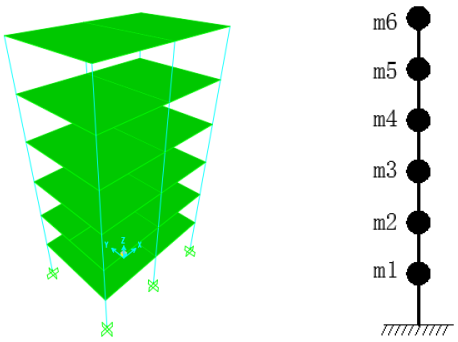

(a) SAP2000 model. (b) 6-DOF equivalent shear model.

Figure 3. The structural model of SAP2000 and the 6-DOF equivalent shear model.

The mass of the structure is mainly concentrated at each floor, which is 3650kg for each floor according to the test structure. Therefore, a 6-DOF equivalent shear model, see Figure 3(b), can be developed to simplify the analysis of the test structure model. The stiffness matrix of the 6-DOF equivalent shear model is obtained according to the model of SAP2000 as

$$\boldsymbol{K} = (\boldsymbol{\Phi}^{\mathrm{T}})^{-1}\boldsymbol{\Omega}(\boldsymbol{\Phi})^{-1} \tag{20}$$

where $\boldsymbol{K}$ is the stiffness matrix; $\boldsymbol{\Phi}$ is the matrix of mode shapes of the model of SAP2000; $\boldsymbol{\Omega}$ is a diagonal matrix with diagonal elements $\omega_i{}^2$, and ω_i is the i^{th} characteristic frequency of the structure in X-direction.

The first four characteristic frequencies are compared in Table 1. The errors are quit small except the fourth characteristic frequency of 6.8% which is still acceptable. Therefore, the 6-DOF equivalent shear

model can be applied instead of the finite element model of SAP2000. The stochastic response analyses, using this model, are implemented for both the base-fixed structure and base-isolated structure combining the PDEM and the stochastic model of seismic ground motions.

Table 1. Comparison of the structural first four order characteristic frequencies.

Mode	**1** Hz	**2** Hz	**3** Hz	**4** Hz
SAP2000	1.76	5.49	11.30	19.10
6 - DOF	1.82	5.69	11.35	17.80
Error	3.4%	3.6%	0.4%	6.8%

In addition, Rayleigh damping is applied in this contribution, and the damping ratio for all models are 0.02. Stochastic seismic response analyses of the structure are carried out in two cases: the base-isolated structure subjected to ground motion under design basic earthquake of intensity 8 (i.e. PGA is 0.2g); and the base-fixed structure subjected to ground motion under design basic earthquake of intensity 7 (i.e. PGA is 0.1g). The PGAs are considered according to the Chinese Code for Seismic Design of Buildings (GB50011-2010). Considering the length of the paper, only part of the results in X-direction will be presented in the following subsections.

5.2 *Stochastic seismic response analysis of base-isolated structure with sliding hydromagnetic bearings*

Combining the isolation theory with the probability density evolution method (PDEM) and the stochastic function model of ground motions, the stochastic seismic response analysis of the base-isolated structure with sliding hydromagnetic bearings are implemented in this subsection.

The power-function model for the restoring force of the sliding hydromagnetic bearing is applied as presented in section 2. Meanwhile, the three hundreds representative artificial seismic ground motions are employed to undertake the stochastic analysis using the equivalent shear model. The extreme values obtained in the stochastic analysis are employed to calculate the mean of the inter-story drift responses of all the stories.

As shown in Figure 4, the mean and standard deviation of typical inter-story drifts are presented when the base-isolated structure subjected to ground motion under design basic earthquake of intensity 8 (i.e. PGA is 0.2g). The mean and standard deviation of the inter-story drifts or displacements of the base story are shown in Figure 4(a). The mean and the standard deviation of the inter-story drift of base story are non-stationary. Moreover, the quantity level of the mean inter-story drift response is around 10% of the standard deviation due to the near-zero mean characteristic of the stochastic ground motions. The standard deviation process presents a stage with larger value in the time interval from 5-60s.

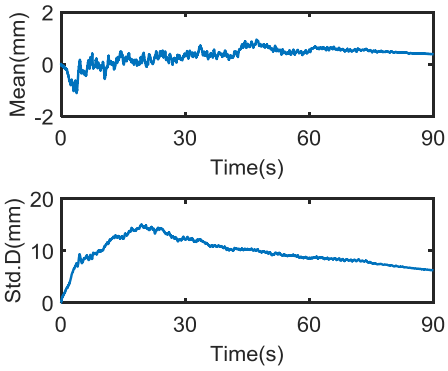

(a) The inter-story drift of the base story.

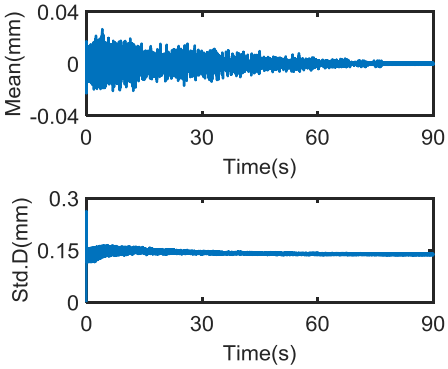

(b) The inter-story drift of the first story.

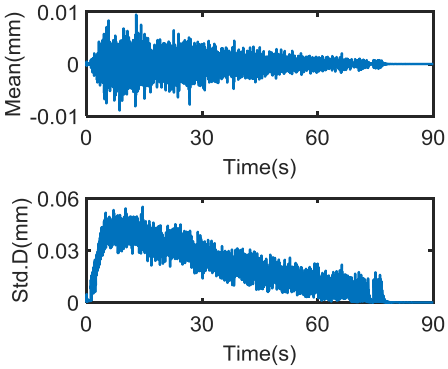

(c) The inter-story drift of the sixth story.

Figure 4. The mean and standard deviation of the inter-story drift responses (0.2g).

Figures 4(b) and 4(c) show the mean and standard deviation of inter-story drifts of the first story and the sixth story, respectively. It is obvious that the mean and standard deviation of the both inter-story drift are much more non-stationary than the values of the base story. The quantity level of the mean inter-story drift responses are around 10% of the standard deviations. However, the standard deviation of the inter-story drifts of the first story remains at around 0.14mm in the time interval from 30-90s, which is quite different with the standard deviations of inter-story drifts of the other five stories, for the influence of relative much smaller stiffness and mass of the base story. In addition, the inter-story drifts of the second to the sixth

stories are in somewhat synchronization except the scales are different, which are similar to that of the sixth story in Figure 4(c).

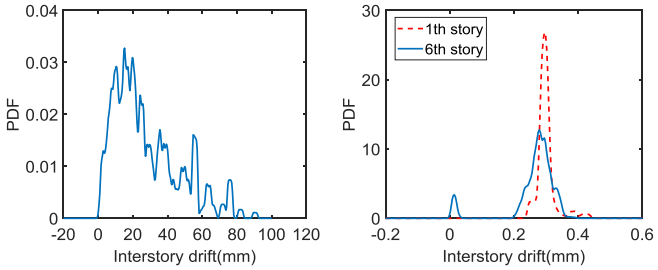

(a) The base story. (b) The first and the sixth story.

Figure 5. The pdfs of the extreme values of the inter-story drift responses (0.2g).

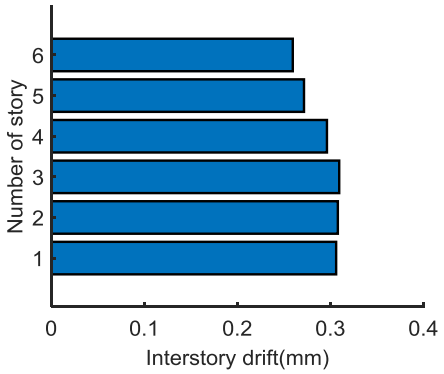

Figure 6. The mean of the extreme values of the inter-story drift responses (0.2g).

In Figure 5 the pdfs of the extreme value (maximum absolute value) of the inter-story drifts of the base story, the first story and the sixth story are presented. The pdfs are irregular, quite different from widely used regular probability distributions. Figure 5(a) shows the pdf of the inter-story drift of the base story. The pdf is quite irregular and varies greatly against the inter-story drift with a large width of the distribution between 0mm and 100mm due to the complex mechanical characteristic of the sliding hydromagnetic. Meanwhile, the pdfs of the inter-story drift of the first and the sixth stories are shown in Figure 5(b). The pdf of the inter-story drift of the first story is concentrated around 0.31mm. However, the pdf of the inter-story drift of the sixth story hasdouble peaks, which is quite different from that of the first story. It can be explained as the influence of the base story which is the same as Figure 4(b). In addition, the first peak is near zero, which means the responses of the superstructure under some stochastic ground motions are quite small.

The mean of the extreme values of different inter-story drifts are presented in Figure 6. Although the upper stories are a little smaller, the mean of the extreme values of different inter-story drifts are almost the same, i.e. around 0.3mm. It means that the superstructure vibrates as a near-rigid body exhibiting obvious elastic behavior.

5.3 *Stochastic seismic response analysis of base-fixed structure*

Combining the probability density evolution method (PDEM) and the stochastic function model of seismic ground motions, the stochastic seismic response analysis of the base-fixed structure are implemented in this subsection. However, the base-fixed structure subjects to ground motion under design basic earthquake of intensity 7 (i.e. PGA is 0.1g).

The 6-DOF equivalent shear model and the three hundreds representative artificial seismic ground motions are employed to carry out the stochastic analysis.

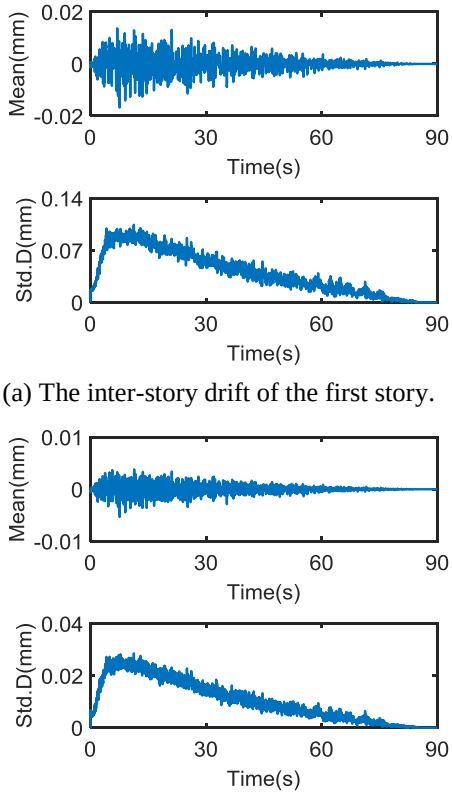

(a) The inter-story drift of the first story.

(b) The inter-story drift of the sixth story.

Figure 7. The mean and standard deviation of the inter-story drift responses (0.1g).

As shown in Figure 7, the mean and standard deviation of typical inter-story drifts are presented. Figures 7(a) and 7(b) show the mean and standard deviation of inter-story drifts of the first story and the sixth story, respectively. It is obvious that the mean and standard deviation of the both inter-story drifts are non-stationary. Comparing to the responses of base-isolated structure in Figure 4, the mean and standard deviation of base-fixed structure are smaller. The quantity level of the mean inter-story drift responses are around 12% of the standard deviations. However, the shape of standard deviations of the first inter-story

drift becomes similar to other stories except the scales are different, see Figure 7(a) and Figure 7(b), which is quite different with the inter-story drifts of base-isolated structure, due to the influence of relatively much smaller stiffness and mass of the base story. However, it should be noted that the shapes of both the mean and standard deviation of inter-story drifts are quite different from that of base-isolated structure, see Figure 4(c) and Figure7.

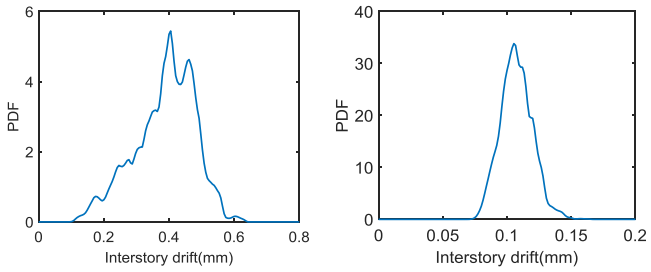

(a) The first story. (b) The sixth story.

Figure 8. The pdfs of the extreme values of the inter-story drift responses (0.1g).

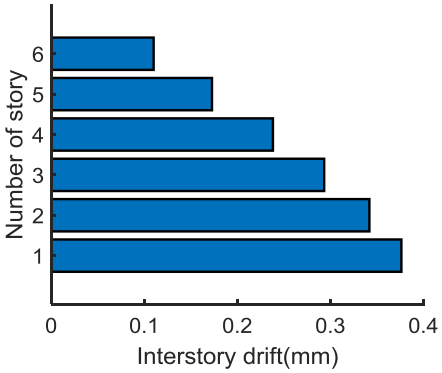

Figure 9. The mean of the extreme values of the inter-story drift responses (0.1g).

In Figure 8 the pdfs of the extreme value (maximum absolute value) of the inter-story drifts of the first story and the sixth story are presented. The pdfs are irregular and don't synchronize for the influence of high-order mode shapes in the corresponding responses. Figure 8(a) shows the pdf of the inter-story drift at the first story. The pdf is quite irregular and varies greatly against the inter-story drift. Meanwhile, the pdf of the inter-story drift of the sixth story is shown in Figure 8(b). The pdf of the inter-story drift of the sixth story is concentrated around 0.12mm which is smaller than pdf of the first story. Although only the pdfs of first story and sixth story are presented here, it is necessary to indicate that the shapes of pdfs of the second story and third story are similar to the shape of pdf of first story. However, the shapes of pdfs of the fourth story and fifth story are similar to the shape of pdf of sixth story.

Compared to the case of the base-isolated structure, it is interesting to find that the distribution of the pdf of the inter-story drifts of the first story is mainly between 0.1mm and 0.5mm. Although the pdf of the base-isolated structure, see Figure 5(b), is mainly between 0.2mm and 0.4mm, most of the extreme values are smaller than the responses of base-fixed structure. However, it is in contrast to that of the sixth story. It can be explained that the supperstructure of base-isolated structure is more like a rigid body, but the base-fixed structure vibrates as a shear model. In addition, it can also be verified by Figure 9.

The mean of the extreme values of different inter-story drifts are presented in Figure 9, which is decreasing with the story number in a linear way. This is quite different from that of the base-isolated structure. It can be explained that the base-isolated structure exhibits obvious elastic behavior. Compared to Figure 6, it is interesting to find that the inter-story of the third story is almost the same with the base-isolated structure, and the first and second stories are larger, but the fourth to the sixth stories are smaller. To the some extent, this indicates that the responses, i.e. the inter-story drifts, of the base-isolated structure are reduced to the level of responses of the base-fixed structure. In addition, the maximum response, i.e. the response of the first story, is less than that of the base-fixed structure. Therefore, the sliding hydromagnetic bearing can achieve the goal of reducing the response by one degree of seismic intensity.

5.4 *Reliability assessment of the base-isolated structure*

The pdfs of the extreme values of inter-story drifts are employed to assess the reliabilities of the base-isolated structure. According to the requirement of seismic design, the inter-story drifts should not exceed the limit state (used as the threshold). The reliability against the inter-story drift of the base story and the reliabilities of upper stories are implemented. The reliability assessment results are listed in Table 3. In this contribution, the limit states for the base story and upper stories are 63.5mm and 3.6mm (i.e. 900/250), respectively.

Table 2. Reliabilities of the inter-story drift responses of the base-isolated structure.

Number	**Threshold***	**Reliability**
Base	63.5 mm	0.946
1	3.6 mm	1.000
2	3.6 mm	1.000
3	3.6 mm	1.000
4	3.6 mm	1.000
5	3.6 mm	1.000
6	3.6 mm	1.000

* Maximum displacement permitted.

From Table 2 it is seen that all the reliabilities of the upper stories are one. However, the reliability of

the base story is 0.946, i.e. the failure probability is 0.054. Therefore, the upper stories of the structure is safe enough, but there exists some risk for the base story. According to these quantified reliabilities, the designer could make a decision whether to implement the present seismic design program or not.

6 CONCLUSIONS

Stochastic response and reliability analysis of the base-isolated structure with sliding hydromagnetic bearings are implemented in detail through combing the physical stochastic function model of ground motions and the probability density evolution method (PDEM). Seismic response of the base-fixed structure is invested to compare to the performance of the base-isolated structure.

Compared to the response of inter-story of the base-fixed structure, the effect of base-isolation with sliding hydromagnetic bearings can reduce the responses by one degree of seismic intensity. In addition, the superstructure of the base-isolated structure vibrates like a rigid body under the seismic ground motions. This indicates the sliding hydromagnetic bearing is efficient in controlling the responses of the structure and can achieve the demanding of seismic protection.

According to reliability assessment of the extreme values of the inter-story drifts of the base-isolated structure, the superstructure is safe enough. However, the reliability of the base story is 0.946, and thus there exists some risk of the inter-story drift or displacement limit being exceeded. The results provide quantified indices for decision making of the designer and the owner.

7 ACKNOWLEDGEMENTS

Financial support from the National Natural Science Foundation of China (NSFC Grant Nos. 11761131014 and 51725804) is gratefully appreciated. The first author would like to thank the China Scholarship Council and the Magnel Laboratory for Concrete Research of Ghent University for the financial support. Further, the help of Dr. Yanqiong Ding for providing the program of generating representative accelerations of the stochastic seismic ground motions is highly appreciated.

8 REFERENCES

Boore, D.M. 1983. Stochastic simulation of high-frequency ground motions based on seismological models of the radiated spectra. *Bulletin of the Seismological Society of America* 73(6A): 1865-1894.

Chen, J.B., Liu, W.Q., Peng, Y.B. & Li, J. 2007. Stochastic seismic response and reliability analysis of base-isolated structures. *Journal of Earthquake Engineering* 11(6): 903-924.

Chen, J.B., Yang, J.Y. & Li, J. 2016. A GF-discrepancy for point selection in stochastic seismic response analysis of structures with uncertain parameters. *Structural Safety* 59: 20-31.

Ding, Y.Q., Peng, Y.B. & Li, J. 2018a. A Stochastic Semi-Physical Model of Seismic Ground Motions in Time Domain. *Journal of Earthquake and Tsunami*: p.1850006.

Ding, Y.Q., Peng, Y.B. & Li, J. 2018b. Cluster Analysis of Earthquake Ground-Motion Records and Characteristic Period of Seismic Response Spectrum. *Journal of Earthquake Engineering*: 1-22.

Erkus, B. & Johnson, E.A. 2006. Smart base-isolated benchmark building Part III: A sample controller for bilinear isolation. *Structural Control & Health Monitoring* 13(2-3): 605-625.

Guo, A.X., Li, Z.J., Li, H. & Ou, J.P. 2009. Experimental and analytical study on pounding reduction of base-isolated highway bridges using MR dampers. *Earthquake Engineering and Structural Dynamics* 38(11): 1307-1333.

Li, J. & Chen, J.B. 2009. *Stochastic dynamics of structures*. Singapore: John Wiley & Sons.

Li, J., Chen, J.B. & Fan, W.L. 2007. The equivalent extreme-value event and evaluation of the structural system reliability. *Structural Safety* 29(2): 112-131.

Narasimhan, S., Nagarajaiah, S., Johnson, E.A. & Gavin, H.P. 2006. Smart base-isolated benchmark building. Part I: problem definition. *Structural Control & Health Monitoring* 13(2-3): 573-588.

Peng, Y.B., Ding, L.C., Shi, J.Y., Chen, J.B. & Villaverde, R. 2017. Experimental study of sliding hydromagnetic isolator for seismic protection. *Journal of Structural Engineering*, under review.

Peng, Y.B., Ding, L.C., Shi, J.Y. & Chen, J.B. 2018. Performance Evaluation of Base-isolated Structures with Sliding Hydromagnetic Bearings. *Journal of Structural Control and Health Monitoring*, under review.

Rezaeian, S. & Der Kiureghian, A. 2008. A stochastic ground motion model with separable temporal and spectral nonstationarities. *Earthquake Engineering & Structural Dynamics* 37(13): 1565-1584.

Saaed, T. E., Nikolakopoulos, G., Jonasson, J. E. & Hedlund, H. 2015. A state-of-the-art review of structural control systems. *Journal of Vibration and Control* 21(5): 919-937.

Villaverde, R. 2017. Base isolation with sliding hydromagnetic bearings: concept and feasibility study. *Structure and Infrastructure Engineering* 13(6): 709-721.

Wang, D. & Li, J. 2011. Physical stochastic function model of ground motions for engineering purposes. *Science China Technological Sciences* 54(1): 175-182.